SHORT COMMUNICATION

Application of machine learning to pretherapeutically estimate dosimetry in men with advanced prostate cancer treated with ^{177}Lu-PSMA I&T therapy

Song Xue[1] · Andrei Gafita[2,3] · Chao Dong[4] · Yu Zhao[5] · Giles Tetteh[5] · Bjoern H. Menze[5] · Sibylle Ziegler[6] · Wolfgang Weber[2] · Ali Afshar-Oromieh[1] · Axel Rominger[1] · Matthias Eiber[2] · Kuangyu Shi[1,5]

Abstract

Purpose Although treatment planning and individualized dose application for emerging prostate-specific membrane antigen (PSMA)-targeted radioligand therapy (RLT) are generally recommended, it is still difficult to implement in practice at the moment. In this study, we aimed to prove the concept of pretherapeutic prediction of dosimetry based on imaging and laboratory measurements before the RLT treatment.

Methods Twenty-three patients with metastatic castration-resistant prostate cancer (mCRPC) treated with ^{177}Lu-PSMA I&T RLT were included retrospectively. They had available pre-therapy ^{68}Ga-PSMA-HEBD-CC PET/CT and at least 3 planar and 1 SPECT/CT imaging for dosimetry. Overall, 43 cycles of ^{177}Lu-PSMA I&T RLT were applied. Organ-based standard uptake values (SUVs) were obtained from pre-therapy PET/CT scans. Patient dosimetry was calculated for the kidney, liver, spleen, and salivary glands using Hermes Hybrid Dosimetry 4.0 from the planar and SPECT/CT images. Machine learning methods were explored for dose prediction from organ SUVs and laboratory measurements. The uncertainty of these dose predictions was compared with the population-based dosimetry estimates. Mean absolute percentage error (MAPE) was used to assess the prediction uncertainty of estimated dosimetry.

Results An optimal machine learning method achieved a dosimetry prediction MAPE of $15.8 \pm 13.2\%$ for the kidney, $29.6\% \pm 13.7\%$ for the liver, $23.8\% \pm 13.1\%$ for the salivary glands, and $32.1 \pm 31.4\%$ for the spleen. In contrast, the prediction based on literature population mean has significantly larger MAPE ($p < 0.01$), $25.5 \pm 17.3\%$ for the kidney, $139.1\% \pm 111.5\%$ for the liver, $67.0 \pm 58.3\%$ for the salivary glands, and $54.1 \pm 215.3\%$ for the spleen.

Conclusion The preliminary results confirmed the feasibility of pretherapeutic estimation of treatment dosimetry and its added value to empirical population-based estimation. The exploration of dose prediction may support the implementation of treatment planning for RLT.

Keywords Radioligand therapy · ^{177}Lu-PSMA I&T · Dosimetry · Treatment planning · Machine learning

---

This article is part of the Topical Collection on Advanced Image Analyses (Radiomics and Artificial Intelligence).

✉ Kuangyu Shi
kuangyu.shi@dbmr.unibe.ch

[1] Dept. Nuclear Medicine, Inselspital, Bern University Hospital, University of Bern, Bern, Switzerland

[2] Dept. Nuclear Medicine, Technical University of Munich, Munich, Germany

[3] Dept. Molecular & Medical Pharmacology, University of California, Los Angeles, CA, USA

[4] Dept. Electrical Engineering, Technical University of Munich, Munich, Germany

[5] Dept. Informatics, Technical University of Munich, Munich, Germany

[6] Dept. Nuclear Medicine, University Hospital, LMU Munich, Munich, Germany

Introduction

Radioligand therapy (RLT) is a contemporary approach to radiation oncology, aiming to deliver the maximal destructive radiation dose via cancer-targeting radiopharmaceutical. Radioactive ligands for the prostate-specific membrane antigen (PSMA) have emerged for the treatment of metastatic castration-resistant prostate cancer (mCRPC) [1–3]. Notably, ^{177}Lu-PSMA-617 was validated recently in a phase III randomized clinical trial [4] which led to the U.S. Food and Drug Administration (FDA) approval [5].

Despite the early success of RLT, concerns have been raised about the risks of inadequate trade-off between therapeutic dose and side effects. Currently, the protocols for administering the radiopharmaceuticals are assessed on a population basis, and the activity to administer was determined for a specific patient group based on preceding studies [6]. However, the European Council Directive (2013/59 Euratom) mandates that RLT treatments should be planned according to the optimal radiation dose tailored for individual patients, as has long been the case for external beam radiotherapy (EBRT) or brachytherapy [7, 8]. An essential requirement of RLT treatment planning is to estimate the absorbed dose in advance of therapy [9, 10].

Prior knowledge of the biodistribution of the therapeutic agent via the pre-therapy imaging assists to optimize the trade-off between tumor destruction and irradiation of healthy tissues [11–15]. Concepts, such as physiologically based pharmacokinetic (PBPK) modeling, have been proposed to estimate the spatiotemporal pharmacokinetics of imaging agents and then extrapolate to the treatment agents [7, 10, 16, 17]. Normal organ and tumor pharmacokinetics can be assessed by a series of cross-sectional whole-body SPECT scans [18]. However, these require a large amount imaging time and are often not feasible in routine clinical practice. An alternative is pharmacokinetic modeling based on the activity concentration in the blood and a computational model which describes the binding of the ligand to its target as well as its metabolism and excretion. However, these models can be numerically unstable [18], thus presenting a dilemma in making a trade-off between numerical stability and physiological fidelity [19]. Due to these technical limitations, the pre-therapy imaging is usually only used in current practice to qualitatively select candidates for RLT and to rule out obvious risks. The patients are still treated with a fixed radiopharmaceutical activity and fraction interval protocol [20, 21].

As illustrated in Fig. 1, our study aimed to prove the concept of dosimetry prediction based on pre-therapy PET imaging and blood test results by providing an alternative solution with machine learning (ML) technique. We aimed to evaluate the feasibility to obtain estimation of the pharmacokinetics of PSMA ligands over several days from a single time point PET scan acquired after 1 h. Such concept would help to avoid a series of whole-body imaging with long procedure scans. Furthermore, it could be directly implemented in the current routine clinical protocol, which may provide a practical solution for dosimetry-based treatment planning for RLT.
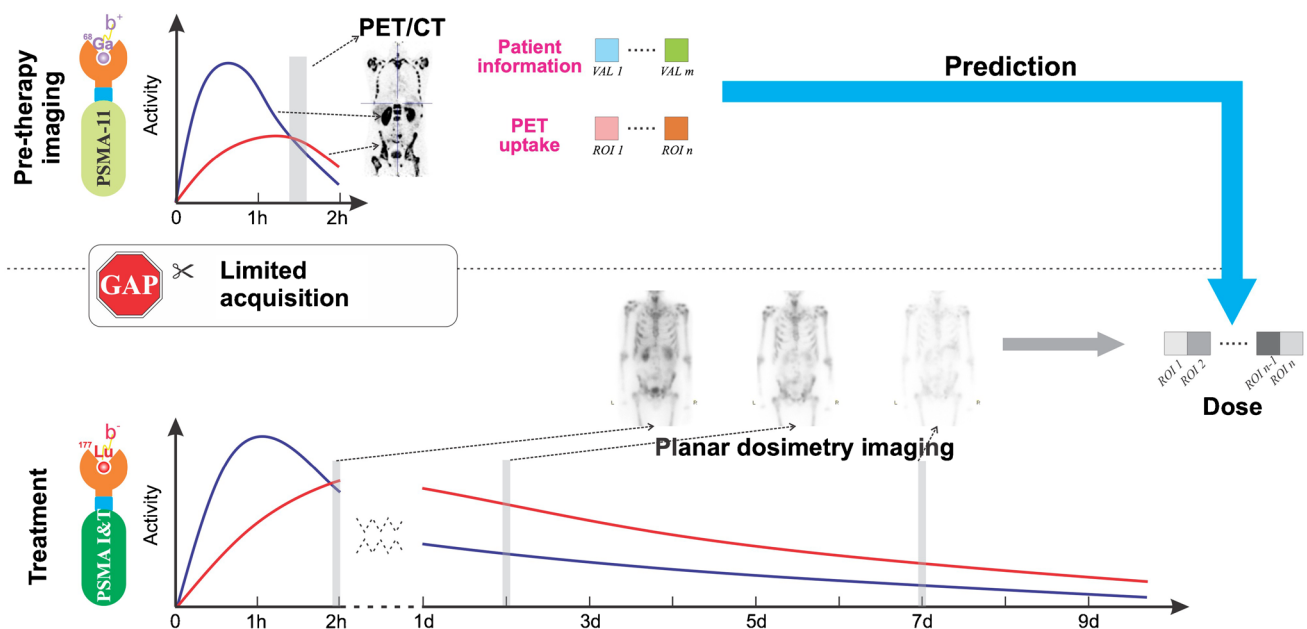

Fig. 1 Illustration of our proposed method; our study aims to prove the concept of individual dosimetry prediction based on pre-therapy imaging and laboratory measurements, by providing an alternative solution with machine learning (ML) technique

Materials and methods

Patient cohorts

Patients with metastatic castration-resistant prostate cancer (mCRPC) who (i) were treated with ^{177}Lu-PSMA I&T RLT at Klinikum rechts der Isar between December 2014 and August 2017, (ii) received pretherapeutic ^{68}Ga-PSMA-HEBD-CC (PSMA-11) PET/CT within 2 months of treatment initiation, and (iii) received at least 3 post-therapeutic planar imaging in conjunction with 1 SPECT/CT were screened retrospectively for inclusion. Twenty-three patients met the eligibility criteria and were included. After image review, 1 patient with invisible liver and spleen on planar PET scan was excluded. Overall, 43 cycles of ^{177}Lu-PSMA I&T RLT were applied (21 first, 11 s, 5 third, and 6 fourth or further cycles). For each cycle, the patients referred to ^{68}Ga-PMSA-HEBD-CC PET/CT for pre-therapy imaging, and less than 2 months later underwent 3–5 planar whole-body scans and SPECT/CT after injecting approximately 7.4 GBq (7.3 ± 0.3 GBq) ^{177}Lu-PSMA I&T, for the purpose of dosimetry investigation. For all subjects, anterior and posterior whole-body scintigraphy was performed at least at three time points, which are 30–150 min, 24 h, and 6–8 days after injection. The retrospective analysis was conducted in accordance with the requirements of the respective local ethics committees in Germany, the institutional review board (IRB) of the Technische Universität München approved this study (IRB reference no: 115/18). All patients signed written informed consent prior to the use of Lu-PSMA as part of a compassionate use application. ^{177}Lu-PSMA I&T was administered in compliance with The German Medicinal Products Act, AMG §13 2b, and in accordance with the responsible regulatory body (Government of Oberbayern).

Image analysis and dosimetry estimation

Our proposed ML-based dose estimation method was designed as a supervised learning approach, which requires labeled training datasets. As shown in Fig. 1, both clinical information of patients and PET imaging data are the inputs to the model, and the corresponding organ-level dosimetry is used as the ground truth for training.

As shown in Table 1, both quantities derived from pre-therapy imaging and blood test results were collected as input for the development of the prediction model. Among them, 11 blood tests results were included such as creatinine, albumin, and lactate dehydrogenase (LDH). As for the features from PET imaging, targeted organs (whole body, kidneys, spleen, liver, parotid glands, and submandibular glands) were delineated manually and reviewed by

board-certified nuclear medicine physicians. Imaging parameters including volume-related features and voxel intensity-related features, as well as standard uptake value (SUV)-related features, were calculated from the targeted organs.

We used Hermes [22] to calculate organ-level dosimetry. Hermes Medical Solutions (HERMES, Stockholm, Sweden) markets a suite of dosimetry tools, including Hybrid Viewer Dosimetry (HVD) and Olinda/EXM, which provides organ-level dosimetry calculation using medical internal radiation dose (MIRD) schema [23]. As shown in Fig. 2, planar whole-body images of five time points as well as one of the SPECT/CT images were loaded into HVD first, and targeted organs were then delineated by 2 board-certified nuclear medicine physicians. Time-integrated activity coefficient (TIAC) was performed by HVD, and residence time was input into the linked Olinda/EXM for dose calculation [24].

Model setup

The dosimetry prediction model was developed with the input of both PET imaging features and clinical features, and the corresponding dosimetry of targeted organ as ground truth. During the training of the model, we tend to optimize the mean squared error loss

$$MSE = \frac{\sum_{i=1}^{n} (y_i - \hat{y}_i)^2}{n}$$

where $\hat{y}_i$ is the predicted absorbed dose that the network assigns to the label i, y_i is the ground truth of each input, and n is the number of input data. ML techniques were recruited for the dose prediction. More information on the model setup is attached in the corresponding part of Supplementary material.

Evaluation

To evaluate the prediction uncertainty of our ML-based model, we compared our estimations with population-based dose using mean absolute percentage error (MAPE). Population-based dose may be estimated empirically before the treatment based on published data. In this study, we considered the mean dosimetry results from population-based dosimetry estimations published previously [25] as a reference. We used a mean absorbed dose of 0.72 Gy/GBq for the kidney and 0.12 Gy/GBq for the liver and the absorbed dose for salivary glands (0.59 Gy/GBq) was averaged over the parotid and submandibular glands. Due to the absence of spleen dose [25], we adopted the average absorbed dose from our own dataset, which was 0.31 Gy/GBq.

Table 1 Recruited clinical features (blood test) and PET features (volume, voxel intensity, and SUV) for the development of our proposed machine learning algorithm

Type of feature	Name of feature	Description
Volume-related features	Vol	Volume of targeted organ
	V40	Percentage volume with at least 40% intensity
	V70	Percentage volume with at least 70% intensity
	V90	Percentage volume with at least 90% intensity
Voxel intensity-related features	Total Voxel	Total amount of voxel
	Mean	Mean intensity value
	Min	Minimum intensity value
	Max	Maximum intensity value
	Sum	Summation of intensity value
	Std. Dev	Standard deviation of intensity value
	Skewness	Measure of the symmetry of the intensity distribution
	Kurtosis	Measure of the shape of the peak of the intensity distribution
	Median	Median intensity value
SUV-related features	SUV peak	Average activity concentration within a 1 cm^3 spherical VOI centered on the "hottest focus" within the tumor image multiplied by the ratio of lean body mass (LBM) to injected activity decayed to time of scan
	SUV mean	Mean SUV value
	SUV min	Minimum SUV value
	SUV max	Maximum SUV value
	SUV TLG	The product of SUV mean and metabolic tumor volume (MTV)
	SUV std. Dev	Standard deviation of SUV value
	SUV median	Median SUV value
Blood tests	Interval	
	Creatinine clearance (ml/min)	
	Alkaline phosphate (ALP) (U/L)	
	Total bilirubin (mg/dL)	
	Lactate dehydrogenase (LDH) (U/L)	
	Albumin (g/L)	
	Prothrombin time (min)	
	Leukocyte count (/L)	
	Hemoglobin (g/L)	
	Thrombocyte count (/L)	
	PSA (µg/L)	

## Results

Time activity curve (TAC) and dosimetry

We used Hermes software to generate the TAC and absorbed dose of each target organ based on planar whole-body and SPECT/CT images. Figure 3 shows an example of a TAC, the left panel shows the change of fraction of injected activity over time of each organ, and the right panel shows the change of fraction of injected activity over time of the whole body. Complete statistics including absorbed dose for all subjects can be found in Table 2. According to both the TAC and Table 2, kidneys represent the critical organ with a mean absorbed dose of 0.65 Gy/GBq. Liver accounts for the largest percentage

of cumulated activity in the entire body and decays at the fastest rate compared to any other organ. In contrast, salivary gland activity remained the smallest proportion of the whole body and decayed more slowly. All curves showed a similar trend of decay after 100 h. Additionally, Supplementary Fig. 4 shows that the greater time interval between each treatment cycle, the absorbed dose of each organ tended to be less correlated.

Model performance

Results of the comparison between ML-based dose estimation with population-based model are shown in Fig. 4. MAPE was used to assess the prediction uncertainty of estimated dosimetry. For kidney, the mean MAPE and standard

Fig. 2 Planar whole-body images of five time points as well as one of the SPECT/CT images. Regions of interest were labeled on the liver, kidneys, spleen, parotid glands, submandibular glands, lacrimal glands, and bladder
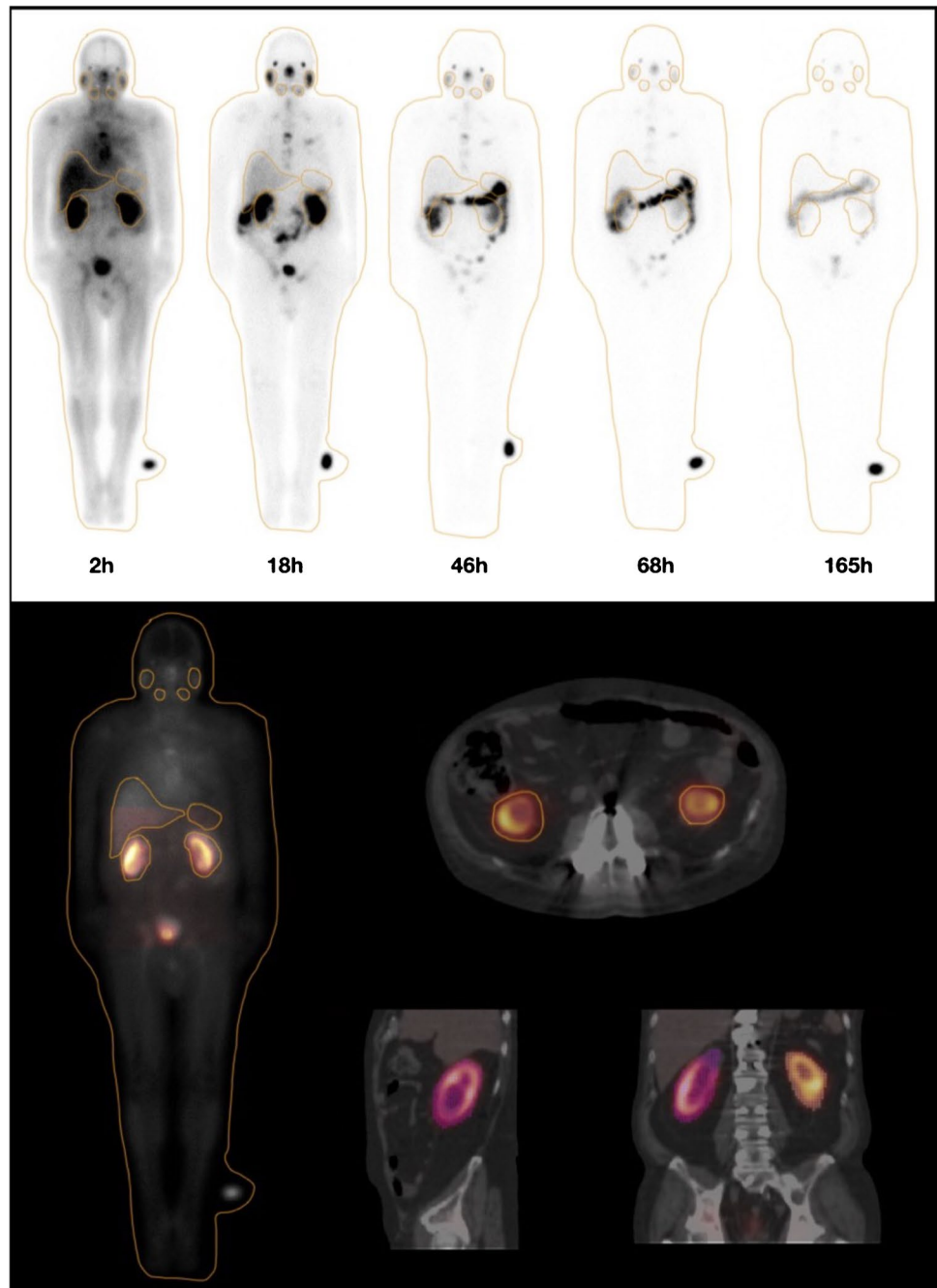
deviation is $15.8\% \pm 13.2\%$. In contrast, population-based MAPE achieved $29.6\% \pm 42.8\%$. For the rest of the organs, the prediction of the liver, spleen, and salivary gland dosimetry achieved $25.5 \pm 17.3\%$, $32.1 \pm 31.4\%$, and $23.8\% \pm 13.1\%$ with ML-based model, and the population-based MAPE is $139.1\% \pm 111.5\%$ for the liver, $54.1 \pm 215.3\%$ for the spleen, and $67.0 \pm 58.3\%$ for the salivary glands. Paired t test showed significant difference between AI prediction and population-based estimation ($p < 0.01$). However, when combining PET imaging features with clinical blood test features, the prediction uncertainty of our model tends to increase in each target

organ, probably for the reason that these features are non-organ-specific. More details of model performance can be found in the corresponding part of Supplementary material.

Discussion

Dose plays a key role in the application of RLT. Current practice of PSMA-directed RLT applies fixed activity to patients. Similar to pharmaceutical practice, the efficacy and risk assessment generally follow the empirical experience

Fig. 3 Example of time activity curve (TAC) generated by Hermes software
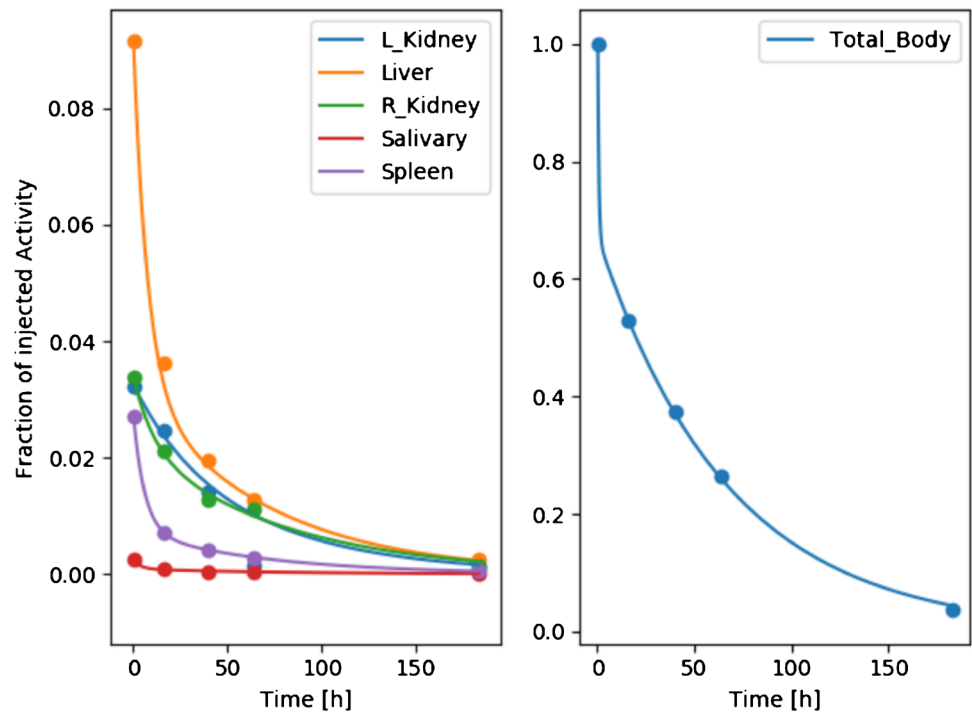

Table 2 Absorbed dose for all subjects of each organ as well as the whole body (in Gy/GBq)

Cycles investigated	Whole body	Kidneys	Liver	Salivary glands	Spleen
Overall (n=43)					
Mean ± SD	0.031 ± 0.017	0.648 ± 0.165	0.067 ± 0.035	0.565 ± 0.389	0.306 ± 0.227
Range	0.012–0.078	0.236–1.041	0.019–0.151	0.150–1.869	0.033–0.918
First cycle (n=21)					
Mean ± SD	0.031 ± 0.016	0.572 ± 0.167	0.060 ± 0.035	0.480 ± 0.269	0.231 ± 0.20
Range	0.012–0.078	0.236–0.820	0.019–0.145	0.150–1.047	0.039–0.715
Second cycle (n=11)					
Mean ± SD	0.033 ± 0.023	0.676 ± 0.266	0.068 ± 0.030	0.596 ± 0.464	0.337 ± 0.395
Range	0.015–0.076	0.314–1.159	0.036–0.128	0.257–1.359	0.033–1.341
Third cycle (n=5)					
Mean ± SD	0.038 ± 0.029	0.753 ± 0.219	0.079 ± 0.033	0.775 ± 0.739	0.570 ± 0.258
Range	0.017–0.059	0.514–1.041	0.048–0.123	0.257–1.869	0.320–0.918
Fourth cycle and further (n=6)					
Mean ± SD	0.033 ± 0.008	0.614 ± 0.172	0.080 ± 0.044	0.602 ± 0.304	0.322 ± 0.272
Range	0.024–0.039	0.328–0.780	0.024–0.151	0.323–1.134	0.046–0.732

[6]. The post-therapy dose distribution can be explicitly or implicitly estimated from cohorts of patients treated with the same protocol in previous studies. These empirical methods function well in clinical practice [26–28]. They enable efficient and economic RLT application and accelerate the clinical translation of novel RLT development. On the other side, RLT is still considered to be an approach to radiation oncology. The experience of external beam radiotherapy recommends the treatment planning to identify the optimal trade-off between therapeutic dose and side effects. Although treatment planning and dose application for RLT are generally recommended by regulatory agencies or scientific societies, no practical solution is available at the moment. Tumor sink effect in ^{68}Ga-PSMA-11 PET imaging was demonstrated previously [29]. These results suggest that candidates for PSMA-RLT with high tumor volume on pretherapeutic PSMA PET might benefit from increased therapeutic activity without exceeding the radiation dose limit for organs at risk.

Pretherapeutic dosimetry estimation is essential to the realization of treatment planning. However, the relationship between pre-therapy imaging and post-therapy dosimetry is
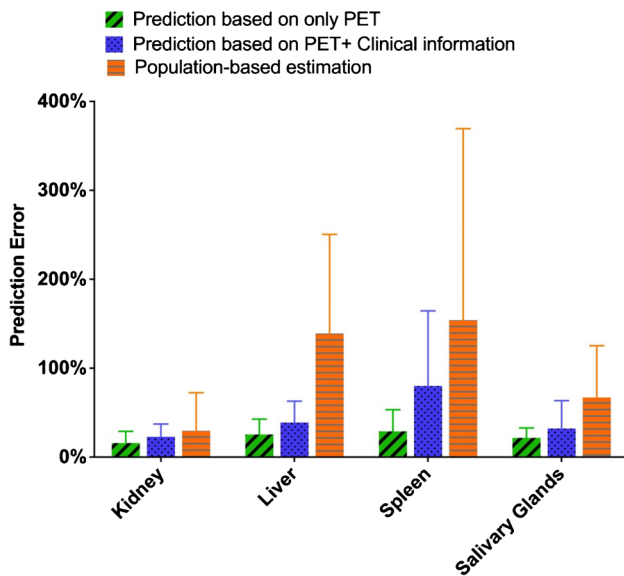
Fig. 4 Comparison of prediction performance between individualized dose estimation with population-based model

complex. The pre-therapy SUV is a single time point uptake measurement after 1 h, while the post-therapy dosimetry is an integration of radiation time course of a similar but not identical tracer over several days. Furthermore, therapeutic tracers (^{177}Lu-PSMA I&T) are injected at several-fold higher activity than imaging tracers (^{68}Ga-PSMA-11), and their ligands are similar but not identical. The theranostic principle of similar pharmacokinetics between the imaging and therapy tracers (PSMA-11 [30] and PSMA I&T [25]) enables the qualitative assessment of the post-therapy dose before the treatment [31]. Previous studies revealed that SUV values of pre-therapy imaging correlate with the post-therapy dose distribution [32, 33]. These correlations confirmed taking into account the pre-treatment information may assist the estimation of the post-therapy dosimetry [34] and reduce the possibilities of under- or over-estimation of different biodistributions [35]. Our preliminary results showed that ML can decrease the uncertainty of this pre-therapeutic dose assessment compared with empirical population-based estimation. The developed ML model took multivariate input and learned quantitative principles from the training data with the regularizations of their underlying interrelations such as multi-organ relative relations [36], which can complement the missing data in prediction. Furthermore, the key question of dosimetry prediction is sort of implicit estimation of the biological half-lives of the therapy tracer from imaging. Previous studies have achieved single time point estimation by assuming that the tissue-specific radioligand uptake curves for different patients are identical [37, 38]. However, as shown in Supplementary Fig. 5, our results showed that the variation of these biological

half-lives between individuals is although relatively small but not negligible (11.2 ± 6.0 h). Our data-driven ML approach modeled for each target organ will better consider the individual variation in the estimation of the absorbed dose. Additionally, Supplementary Fig. 6 shows that of the features extracted from pre-treatment PET imaging, SUV_{max} and tumor volume are most relevant to dose estimation.

Dosimetry methods have been established in the last decades to calculate the dose distribution of the applied therapeutic agents based on a series of planar or 3D images [39–47], which can be used to quantify the whole-body dosimetry of the therapeutic agent. The series of scintigraphy were taken at different time points to sufficiently cover the kinetics of the radiopharmaceutical. The Hermes tool recruited in our study was developed based on MIRD system [23, 39, 48], which is recommended by the European Association of Nuclear Medicine Dosimetry Committee Guidelines. In addition to a series of scintigraphy, we included at least one SPECT/CT for the reason of determining the overall calibration factor of the system sensitivity, which helped to convert the counts of scintigraphy (cts) to the activity concentration of Bq (per voxel). The recommendation of MIRD committee for calibration required extra phantom acquisitions [49], which was not feasible in our study. Inspired by Halty et al. [50], the fraction of activity in each organ was proposed to compute the calibration factor as the total number of counts in the SPECT image divided by this activity derived from the TAC.

There are several limitations of our study. The first is the inherent bias in the limited datasets, and the inclusion of additional subjects may further improve the generalizability and robustness of the developed model. Although the developed ML methods have demonstrated the potential to dissect the complex relation behind the correlation for dosimetry prediction, the limited data for training may limit its prediction power. Training and validation with additional data is necessary to improve the trustworthiness of the dose estimation based on ML. However, to the best of our knowledge, we are the first group to explore the feasibility of estimation of post-therapy dosimetry for ^{177}Lu-PSMA I&T therapy; hence, the availability of these datasets is rather limited at this stage. For the second limitation, the *S* values applied by organ-level dose calculation tools like Olinda/EXM were obtained based on reference phantoms, which were not intended for individualized estimation, which would then result in the inclusion of inaccurate absorbed dose values in our ML model development. Potential uncertainty can occur both for volumetric assessment and SUV measurement for organs. Another limitation of our study is the absence of dose prediction for tumor lesions, which is due to the unavailability of the lesion phantom in the current version of Hermes tool. A similar problem occurred in the attempt to delineate the parotid and submandibular glands separately,

which failed due to the absence of the corresponding phantom. We solved this problem by treating the parotid and submandibular glands as two parts of the salivary gland, which was provided as a phantom in Hermes.

Conclusion

The preliminary results confirmed the feasibility of pretherapeutic dose estimation before the PSMA-RLT and its added value compared with empirical population-based estimation ($p < 0.01$); ML may decrease the estimation uncertainty of post-therapy dosimetry, with an average MAPE of 15.76% for critical dose-absorbing organs (i.e., kidneys). The exploration of dose prediction may support the identification of the role of treatment planning for RLT.

References

1. Ahmadzadehfar H, Schlolaut S, Fimmers R, Yordanova A, Hirzebruch S, Schlenkhoff C, et al. Predictors of overall survival in metastatic castration-resistant prostate cancer patients receiving [177Lu] Lu-PSMA-617 radioligand therapy. Oncotarget Impact J, LLC. 2017;8:103108.

2. Rahbar K, Bögemann M, Ahmadzadehfar H. ^ sup 177^ Lu-PSMA-617 radioligand therapy of mCRPC: evaluation criteria of response. Eur J Nucl Med Mol Imaging Springer Nature BV. 2017;44:166.

3. Fendler WP, Reinhardt S, Ilhan H, Delker A, Böning G, Gildehaus FJ, et al. Preliminary experience with dosimetry, response and patient reported outcome after 177Lu-PSMA-617 therapy for metastatic castration-resistant prostate cancer. Oncotarget Impact J LLC. 2017;8:3581.

4. Sartor O, de Bono J, Chi KN, Fizazi K, Herrmann K, Rahbar K, et al. Lutetium-177–PSMA-617 for Metastatic Castration-Resistant Prostate Cancer. N Engl J Med. Mass Medical Soc; 2021;

5. FDA approves Pluvicto for metastatic castration-resistant prostate cancer [Internet]. Available from: https://www.fda.gov/drugs/ resources-information-approved-drugs/fda-approves-pluvicto-metastatic-castration-resistant-prostate-cancer

6. Hardiansyah D, Maass C, Attarwala AA, Müller B, Kletting P, Mottaghy FM, et al. The role of patient-based treatment planning in peptide receptor radionuclide therapy. Eur J Nucl Med Mol Imaging. Germany; 2016;43:871–80

7. Stokke C, Gabiña PM, Solný P, Cicone F, Sandström M, Gleisner KS, et al. Dosimetry-based treatment planning for molecular radiotherapy: a summary of the 2017 report from the Internal Dosimetry Task Force. EJNMMI Phys SpringerOpen. 2017;4:1–9.

8. Podder TK, Fredman ET, Ellis RJ. Advances in radiotherapy for prostate cancer treatment. Adv Exp Med Biol United States. 2018;1096:31–47.

9. Sgouros G, Bolch WE, Chiti A, Dewaraja YK, Emfietzoglou D, Hobbs RF, et al. ICRU REPORT 96, Dosimetry-Guided Radiopharmaceutical Therapy. J ICRU [Internet]. 2021;21:1–212. https://doi.org/10.1177/14736691211060117 (**Available from**).

10. Erdi AK, Erdi YE, Yorke ED, Wessels BW. Treatment planning for radio-immunotherapy. Phys Med Biol. 1996;41:2009 (**IOP Publishing**).

11. Ahmadzadehfar H, Essler M, Rahbar K, Afshar-Oromieh A. Radionuclide therapy for bone metastases: utility of scintigraphy and PET imaging for treatment planning. PET Clin Elsevier. 2018;13:491–503.

12. Baechler S, Hobbs RF, Boubaker A, Buchegger F, He B, Frey EC, et al. Three-dimensional radiobiological dosimetry of kidneys for treatment planning in peptide receptor radionuclide therapy. Med Phys Wiley Online Library. 2012;39:6118–28.

13. Calais J, Kishan AU, Cao M, Fendler WP, Eiber M, Herrmann K, et al. Potential impact of 68Ga-PSMA-11 PET/CT on prostate cancer definitive radiation therapy planning. J Nucl Med. Soc Nuclear Med; 2018;jnumed-118.

14. Baum RP, Kulkarni HR. THERANOSTICS: from molecular imaging using Ga-68 labeled tracers and PET/CT to personalized radionuclide therapy-the Bad Berka experience. Theranostics. 2012;2:437 (**Ivyspring International Publisher**).

15. Kulkarni HR, Baum RP. Theranostics with Ga-68 somatostatin receptor PET/CT: monitoring response to peptide receptor radionuclide therapy. PET Clin. 2013;9:91–7.

16. Menda Y, Madsen MT, O'Dorisio TM, Sunderland JJ, Watkins GL, Dillon JS, et al. 90Y-DOTATOC dosimetry–based personalized peptide receptor radionuclide therapy. J Nucl Med Soc Nuclear Med. 2018;59:1692–8.

17. Kletting P, Kull T, Maaß C, Malik N, Luster M, Beer AJ, et al. Optimized peptide amount and activity for 90Y-labeled DOTA-TATE therapy. J Nucl Med Soc Nuclear Med. 2016;57:503–8.

18. Carson RE. Precision and accuracy considerations of physiological quantitation in PET. J Cereb Blood Flow Metab. 1991;11:45–50 (**SAGE Publications Sage UK: London, England**).

19. Shi K, Maftei C, Bayer C, Astner S, Gaertner F, Vaupel P, et al. Quantitative analysis of [18F] FMISO PET for tumor hypoxia: correlation with results using immunohistochemistry. Soc Nuclear Med; 2012.

20. Flux GD, Gleisner KS, Chiesa C, Lassmann M, Chouin N, Gear J, et al. From fixed activities to personalized treatments in radionuclide therapy: lost in translation? Eur J Nucl Med Mol Imaging. Springer. 2018;45:152–4.

21. Chiesa C, Gleisner KS, Flux G, Gear J, Walrand S, Bacher K, et al. The conflict between treatment optimization and registration of radiopharmaceuticals with fixed activity posology in oncological nuclear medicine therapy. Springer; 2017.

22. Hippeläinen ET, Tenhunen MJ, Mäenpää HO, Heikkonen JJ, Sohlberg AO. Dosimetry software Hermes Internal Radiation Dosimetry: from quantitative image reconstruction to voxel-level absorbed dose distribution. Nucl Med Commun Wolters Kluwer. 2017;38:357–65.

23. Bolch WE, Eckerman KF, Sgouros G, Thomas SR. MIRD pamphlet no. 21: a generalized schema for radiopharmaceutical dosimetry—standardization of nomenclature. J Nucl Med Soc Nuclear Med. 2009;50:477–84.

24. Stabin MG, Sparks RB, Crowe E. OLINDA/EXM: the second-generation personal computer software for internal dose assessment in nuclear medicine. J Nucl Med United States. 2005;46:1023–7.

25. Okamoto S, Thieme A, Allmann J, D'Alessandria C, Maurer T, Retz M, et al. Radiation dosimetry for (177)Lu-PSMA I&T in metastatic castration-resistant prostate cancer: absorbed dose in normal organs and tumor lesions. J Nucl Med United States. 2017;58:445–50.

26. Tennvall J, Fischer M, Delaloye AB, Bombardieri E, Bodei L, Giammarile F, et al. EANM procedure guideline for radio-immunotherapy for B-cell lymphoma with 90 Y-radiolabelled ibritumomab tiuxetan (Zevalin). Eur J Nucl Med Mol Imaging Springer. 2007;34:616–22.

27. Luster M, Clarke SE, Dietlein M, Lassmann M, Lind P, Oyen WJG, et al. Guidelines for radioiodine therapy of differentiated thyroid cancer. Eur J Nucl Med Mol Imaging Springer. 2008;35:1941–59.

28. Schaefer-Cutillo J, Friedberg JW, Fisher RI. Novel concepts in radioimmunotherapy for non-Hodgkin's lymphoma. Oncol (willist Park NY). 2007;21:203–12.

29. Gafita A, Wang H, Robertson A, Armstrong WR, Zaum R, Weber M, et al. Tumor sink effect in 68Ga-PSMA-11 PET: myth or reality? J Nucl Med Soc Nuclear Med. 2022;63:226–32.

30. Afshar-Oromieh A, Malcher A, Eder M, Eisenhut M, Linhart HG, Hadaschik BA, et al. PET imaging with a [68Ga] gallium-labelled PSMA ligand for the diagnosis of prostate cancer: biodistribution in humans and first evaluation of tumour lesions. Eur J Nucl Med Mol Imaging Springer. 2013;40:486–95.

31. Fendler WP, Eiber M, Beheshti M, Bomanji J, Ceci F, Cho S, et al. (68)Ga-PSMA PET/CT: Joint EANM and SNMMI procedure guideline for prostate cancer imaging: version 1.0. Eur J Nucl Med Mol Imaging Germany. 2017;44:1014–24.

32. Ezziddin S, Lohmar J, Yong-Hing CJ, Sabet A, Ahmadzadehfar H, Kukuk G, et al. Does the pretherapeutic tumor SUV in 68Ga DOTATOC PET predict the absorbed dose of 177Lu octreotate? Clin Nucl Med LWW. 2012;37:e141–7.

33. Hänscheid H, Sweeney RA, Flentje M, Buck AK, Löhr M, Samnick S, et al. PET SUV correlates with radionuclide uptake in peptide receptor therapy in meningioma. Eur J Nucl Med Mol Imaging Springer. 2012;39:1284–8.

34. Lassmann M, Chiesa C, Flux G, Bardiès M. EANM Dosimetry Committee guidance document: good practice of clinical dosimetry reporting. Eur J Nucl Med Mol Imaging Germany. 2011;38:192–200.

35. Glatting G, Bardiès M, Lassmann M. Treatment planning in molecular radiotherapy. Z Med Phys Germany. 2013;23:262–9.

36. Cerrolaza JJ, Picazo ML, Humbert L, Sato Y, Rueckert D, Ballester MÁG, et al. Computational anatomy for multi-organ analysis in medical imaging: a review. Med Image Anal Elsevier. 2019;56:44–67.

37. Plyku D, Hobbs RF, Huang K, Atkins F, Garcia C, Sgouros G, et al. Recombinant human thyroid-stimulating hormone versus thyroid hormone withdrawal in (124)I PET/CT-based dosimetry for (131)I therapy of metastatic differentiated thyroid cancer. J Nucl Med. 2017;58:1146–54.

38. Peters SMB, Hofferber R, Privé BM, de Bakker M, Gotthardt M, Janssen M, et al. [(68)Ga]Ga-PSMA-11 PET imaging as a predictor for absorbed doses in organs at risk and small lesions in [(177)Lu]Lu-PSMA-617 treatment. Germany: Eur J Nucl Med Mol Imaging; 2021.

39. Ljungberg M, Celler A, Konijnenberg MW, Eckerman KF, Dewaraja YK, Sjögreen-Gleisner K. MIRD pamphlet no. 26: joint EANM/MIRD guidelines for quantitative 177Lu SPECT applied for dosimetry of radiopharmaceutical therapy. J Nucl Med Soc Nuclear Med. 2016;57:151–62.

40. Bardiès M, Flux G, Lassmann M, Monsieurs M, Savolainen S, Strand S-E. Quantitative imaging for clinical dosimetry. Nucl Instruments Methods Phys Res Sect A Accel Spectrometers, Detect Assoc Equip. Elsevier; 2006;569:467–71.

41. Brolin G, Gustafsson J, Ljungberg M, Gleisner KS. Pharmacokinetic digital phantoms for accuracy assessment of image-based dosimetry in 177Lu-DOTATATE peptide receptor radionuclide therapy. Phys Med Biol. 2015;60:6131 (**IOP Publishing**).

42. Celler A, Grimes J, Shcherbinin S, Piwowarska-Bilska H, Birkenfeld B. Personalized image-based radiation dosimetry for routine clinical use in peptide receptor radionuclide therapy: pretherapy experience. Theranostics, Gall Other Radionuclides. Springer; 2013;497–517.

43. Ljungberg M, Gleisner KS. Personalized dosimetry for radionuclide therapy using molecular imaging tools. Biomedicines. 2016;4:25 (**Multidisciplinary Digital Publishing Institute**).

44. Werner RA, Weich A, Kircher M, Solnes LB, Javadi MS, Higuchi T, et al. The theranostic promise for neuroendocrine tumors in the late 2010s-where do we stand, where do we go? Theranostics. 2018;8:6088 (**Ivyspring International Publisher**).

45. Furhang EE, Chui CS, Kolbert KS, Larson SM, Sgouros G. Implementation of a Monte Carlo dosimetry method for patient-specific internal emitter therapy. Med Phys Wiley Online Library. 1997;24:1163–72.

46. Hofman MS, Violet J, Hicks RJ, Ferdinandus J, Thang SP, Akhurst T, et al. [177Lu]-PSMA-617 radionuclide treatment in patients with metastatic castration-resistant prostate cancer (LuPSMA trial): a single-centre, single-arm, phase 2 study. Lancet Oncol Elsevier. 2018;19:825–33.

47. Sandström M, Garske U, Granberg D, Sundin A, Lundqvist H. Individualized dosimetry in patients undergoing therapy with (177)Lu-DOTA-D-Phe (1)-Tyr (3)-octreotate. Eur J Nucl Med Mol Imaging Germany. 2010;37:212–25.

48. Watson EE, Stabin MG, Siegel JA. MIRD formulation. Med Phys. 1993;20:511–4.

49. Dewaraja YK, Frey EC, Sgouros G, Brill AB, Roberson P, Zanzonico PB, et al. MIRD pamphlet No 23: quantitative SPECT for patient-specific 3-dimensional dosimetry in internal radionuclide therapy. J Nucl Med. 2012;53:1310–25.

50. Halty A, Badel J-N, Kochebina O, Sarrut D. Image-based SPECT calibration based on the evaluation of the Fraction of Activity in the Field of View. EJNMMI Phys. 2018;5:11.